

New methods for B meson decay constants and form factors from lattice NRQCD

C. Hughes,^{1,2,*} C. T. H. Davies,^{3,†} and C. J. Monahan^{4,5}

(HPQCD Collaboration)[‡]

¹*Fermi National Accelerator Laboratory, Batavia, Illinois 60510, USA*

²*Department of Applied Mathematics and Theoretical Physics, University of Cambridge, Cambridge CB3 0WA, United Kingdom*

³*SUPA, School of Physics and Astronomy, University of Glasgow, Glasgow G12 8QQ, United Kingdom*

⁴*Institute for Nuclear Theory, University of Washington, Seattle, Washington 98195, USA*

⁵*New High Energy Theory Center and Department of Physics and Astronomy, Rutgers, The State University of New Jersey, 136 Frelinghuysen Road, Piscataway, New Jersey 08854, USA*



(Received 6 December 2017; published 20 March 2018)

We determine the normalization of scalar and pseudoscalar current operators made from nonrelativistic b quarks and highly improved staggered light quarks in lattice quantum chromodynamics (QCD) through $\mathcal{O}(\alpha_s)$ and Λ_{QCD}/m_b . We use matrix elements of these operators to extract B meson decay constants and form factors, and then compare to those obtained using the standard vector and axial-vector operators. This provides a test of systematic errors in the lattice QCD determination of the B meson decay constants and form factors. We provide a new value for the B and B_s meson decay constants from lattice QCD calculations on ensembles that include u , d , s , and c quarks in the sea and those that have the u/d quark mass going down to its physical value. Our results are $f_B = 0.196(6)$ GeV, $f_{B_s} = 0.236(7)$ GeV, and $f_{B_s}/f_B = 1.207(7)$, agreeing well with earlier results using the temporal axial current. By combining with these previous results, we provide updated values of $f_B = 0.190(4)$ GeV, $f_{B_s} = 0.229(5)$ GeV, and $f_{B_s}/f_B = 1.206(5)$.

DOI: [10.1103/PhysRevD.97.054509](https://doi.org/10.1103/PhysRevD.97.054509)

I. INTRODUCTION

Hadronic weak decay matrix elements containing b quarks that are calculated in lattice quantum chromodynamics (QCD) are critical to the flavor physics program of overdetermining the Cabibbo-Kobayashi-Maskawa (CKM) matrix in order to find signs of new physics. The accuracy of the lattice QCD results often limits the accuracy with which the CKM matrix elements can be determined and with which the associated unitarity tests can be performed [1]. It is therefore important both to improve and to test the accuracy of the lattice QCD results. This includes determining the lattice QCD values using a variety of different

formalisms for b quarks and light quarks, in addition to using different methodologies within a given formalism.

It is now becoming possible to study heavy quarks up to the mass of the bottom quark using relativistic formalisms [2,3], but this is relatively expensive numerically. Consequently, to date, the most extensive studies of heavy quarks in lattice QCD have been done with nonrelativistic formalisms, such as NonRelativistic Quantum Chromodynamics (NRQCD) [4] or the Fermilab formalism [5] and its variants [6]. Relativistic formalisms have the advantage of simple continuumlike current operators that couple to the W boson that can be chosen to be absolutely normalized, for example through the existence of a partially conserved axial current (PCAC) relation [7]. The main issue with these formalisms is then controlling discretization errors [8]. In nonrelativistic formalisms the numerical calculation itself is more tractable, along with the control of discretization errors, but the current operators have a nonrelativistic expansion and must have their normalization matched to that of the appropriate continuum operator. The expansion and the normalization are the main sources of systematic uncertainty in these lattice QCD results. The

*chughes@fnal.gov

†christine.davies@glasgow.ac.uk

‡<http://www.physics.gla.ac.uk/HPQCD>

Published by the American Physical Society under the terms of the [Creative Commons Attribution 4.0 International license](https://creativecommons.org/licenses/by/4.0/). Further distribution of this work must maintain attribution to the author(s) and the published article's title, journal citation, and DOI. Funded by SCOAP³.

comparison of lattice QCD values derived using non-relativistic and relativistic formalisms provides a test of systematic uncertainties (see, for example, [3,9]). However, it is also important to provide tests of systematic uncertainties within a given formalism using different methods. Here we provide such a test of the NRQCD approach by normalizing new sets of current operators that have not been used in this formalism before, and then comparing results for the decay constants and form factors obtained to the previous determinations.

The archetypal heavy meson weak decay process is annihilation of a B meson to $\tau\nu$. The hadronic parameter which controls the rate of this process is the B meson decay constant, proportional to the matrix element to create a B meson from the vacuum with the temporal axial current containing a heavy quark field and a light antiquark field. The most precise calculation to date of the B meson decay constant, f_B , uses improved lattice NRQCD and highly improved staggered light quarks on gluon field configurations that include u , d , s , and c quarks in the sea with multiple values of the lattice spacing and a u/d quark mass going down to the physical point [9]. That calculation used lattice QCD perturbation theory [10] to normalize the temporal axial current operator through $\mathcal{O}(\alpha_s)$, $\mathcal{O}(\alpha_s\Lambda_{\text{QCD}}/m_b)$, and $\mathcal{O}(\alpha_s a\Lambda_{\text{QCD}})$ and obtained a final uncertainty of 2%, including uncertainties from current operator matching and missing higher order current operators.

Decay constants can also be defined in continuum QCD from pseudoscalar current operators using the PCAC relation. This is typically the method of choice for lattice QCD calculations using relativistic formalisms where a lattice PCAC relation allows the pseudoscalar current to be absolutely normalized. This enables the D and D_s decay constants to be obtained with 0.5% uncertainties using the highly improved staggered quarks (HISQ) formalism [7,11,12]. Here we normalize the NRQCD-light pseudoscalar current through $\mathcal{O}(\alpha_s)$, $\mathcal{O}(\alpha_s\Lambda_{\text{QCD}}/m_b)$, and $\mathcal{O}(\alpha_s a\Lambda_{\text{QCD}})$ and obtain a value for f_B with similar uncertainty to that determined from the temporal axial current, providing a test of the systematic errors.

B meson exclusive semileptonic processes are important for the determination of CKM matrix elements through the matching of experimental decay rates to theoretical expectations as a function of momentum transfer. Here the hadronic parameters that encapsulate the information needed on QCD effects are the form factors, calculable in lattice QCD. For the case in which both initial and final mesons are pseudoscalars (e.g. $B \rightarrow \pi\ell\nu$) there are two form factors, a vector form factor, and a scalar form factor. It is the vector form factor that gives the decay rate in the light lepton mass limit, but both form factors appear in the lattice QCD determination of the matrix elements of the vector current. The form factors can be separated by comparing spatial and temporal vector current matrix elements, but additional information can also be obtained

by determining the scalar form factor directly from the scalar current. Indeed this method has been used for the accurate determination of D and K meson semileptonic form factors in lattice QCD using the HISQ formalism [13–15]. Here we compare results using NRQCD-light scalar currents to those obtained using vector currents for $B \rightarrow \pi\ell\nu$. We discuss how this method will be used in improved “second generation” B meson semileptonic form factor calculations now underway.

The paper is organized as follows: in Sec. II we derive the normalization of the NRQCD-light scalar and pseudo-scalar current operators; in Sec. III we combine this with the lattice calculation of the matrix elements of different components of the current to give results for decay constants and form factors; Sec. IV gives our conclusions, including planned future work using these results.

II. NORMALIZATION OF LATTICE NRQCD CURRENT OPERATORS

Here we discuss the normalization of the lattice NRQCD-HISQ current operators when the light quark is taken to be massless and follow the methodology laid out in [16,17], along with most of the notation. We will start with a discussion of the temporal axial current and show the modifications that need to be made to those results to yield the normalization of the pseudoscalar current. Results for the temporal vector/scalar case are then identical because of the chiral symmetry of the HISQ action.

The matrix element of the appropriate temporal axial current defined in continuum QCD between the vacuum and pseudoscalar meson, H , at rest yields the meson decay constant, f_H , via the relation

$$\langle 0|A_0|H\rangle = f_H M_H, \quad (1)$$

where M_H is the meson mass. The continuum QCD current operator can be systematically expanded in terms of lattice NRQCD-HISQ current operators (whose matrix elements can be determined in a lattice QCD calculation) as

$$A_0 = \sum_j C_{j,A_0}(\alpha_s, am_b) J_{A_0,\text{lat}}^{(j)}, \quad (2)$$

where increasing j corresponds to operators that are higher order in a relativistic expansion. The C_j are dimensionless coefficients that compensate for the different ultraviolet behavior between the continuum and lattice regularizations of QCD, and hence they can be calculated in perturbation theory as a power series in the strong coupling constant, α_s . The coefficients of powers of α_s will depend on the bare heavy quark mass in lattice units, am_b , which is the parameter appearing in the lattice NRQCD action (we use b as the bare mass subscript rather than the generic label h since, in our lattice calculations, this is always the b quark mass). Here we work through $\mathcal{O}(\alpha_s)$ and include the three

operators ($j = 0, 1, 2$) that allow us to match the current through $\mathcal{O}(\alpha_s \Lambda_{\text{QCD}}/m_b)$ and $\mathcal{O}(\alpha_s a \Lambda_{\text{QCD}})$. The determination of the C_j is done most conveniently by choosing to match matrix elements of the left- and right-hand sides of Eq. (2) for a heavy quark to light quark scattering process induced by the current. The procedure then [16,17] is as follows:

- (i) calculate the amplitude for such a process through $\mathcal{O}(\alpha_s)$ in continuum QCD;
- (ii) expand this amplitude through first order in powers of $1/M$ where M is the heavy quark pole mass;
- (iii) choose lattice NRQCD-HISQ operators that reproduce the terms in this expansion and calculate the one-loop mixing matrix of these operators in lattice QCD perturbation theory using the same infrared regulation procedure as used in the continuum. Infrared divergences must cancel between the continuum and lattice calculations in the end, since the two only differ in ultraviolet physics. Note also that the mixing matrix should be calculated at a pole mass that matches that of the continuum calculation;
- (iv) invert this mixing matrix to determine the (finite) C_j coefficients that will give the correct linear combination of lattice currents to produce the same one-loop scattering amplitude as in continuum QCD.

The continuum calculation for the temporal axial current $\bar{q}(x)\gamma_5\gamma_0 h(x)$ was done in [16] in the $\overline{\text{MS}}$ scheme using Feynman gauge, on-shell mass and wave-function renormalization, and a gluon mass (λ) to regulate infrared divergences. $q(x)$ is the light quark field and $h(x)$ the heavy quark field satisfying the Dirac equation, and the γ matrices are the standard ones in Euclidean space-time. The key diagram to be calculated in continuum QCD is shown in Fig. 1, where the double line represents an incoming heavy quark of momentum p , the single line represents an outgoing massless quark of momentum p' , and the cross represents the current. The self-energy diagram must also be evaluated to determine the wave-function renormalization. The result for the temporal axial current amplitude is given through $1/M$ as a combination of five matrix

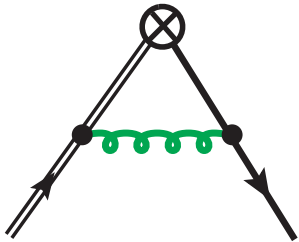


FIG. 1. The Feynman diagram for the vertex renormalization in continuum QCD perturbation theory. The heavy quark is denoted by a double line, the light quark by a single line, and the exchange of a gluon by a curly line. The current is denoted by a cross inside a circle.

elements of Dirac spinors multiplied by factors of p_0 , p'_0 , and $p \cdot p'$ in [16]. By using the Dirac equation for the light quark, and expanding the heavy quark energy and Dirac spinor to $1/M$, this is reduced to

$$\langle q(p')|A_0|h(p)\rangle_{\text{QCD}} = \eta_{A_0}^{(0)} \Omega_{A_0}^{(0)} + \eta_{A_0}^{(1)} \Omega_{A_0}^{(1)} + \eta_{A_0}^{(2)} \Omega_{A_0}^{(2)}. \quad (3)$$

The coefficients are

$$\begin{aligned} \eta_{A_0}^{(0)} &= 1 + \alpha_s B_{A_0}^{(0)}, \\ \eta_{A_0}^{(1)} &= 1 + \alpha_s B_{A_0}^{(1)}, \\ \eta_{A_0}^{(2)} &= \alpha_s B_{A_0}^{(2)} \end{aligned} \quad (4)$$

with

$$\begin{aligned} B_{A_0}^{(0)} &= \frac{1}{3\pi} \left[3 \ln \frac{M}{\lambda} - \frac{3}{4} \right], \\ B_{A_0}^{(1)} &= \frac{1}{3\pi} \left[3 \ln \frac{M}{\lambda} - \frac{19}{4} \right], \\ B_{A_0}^{(2)} &= \frac{1}{3\pi} \left[12 - \frac{16\pi M}{3\lambda} \right]. \end{aligned} \quad (5)$$

The constituent matrix elements are

$$\begin{aligned} \Omega_{A_0}^{(0)} &= \bar{u}_q(p') \gamma_5 \gamma_0 u_Q(p), \\ \Omega_{A_0}^{(1)} &= -i \bar{u}_q(p') \gamma_5 \gamma_0 \frac{\boldsymbol{\gamma} \cdot \mathbf{p}}{2M} u_Q(p), \\ \Omega_{A_0}^{(2)} &= i \bar{u}_q(p') \frac{\boldsymbol{\gamma} \cdot \mathbf{p}'}{2M} \gamma_0 \gamma_5 \gamma_0 u_Q(p), \end{aligned} \quad (6)$$

where u_Q is a two-component spinor related to the Dirac spinor $u_h(p)$ [to $\mathcal{O}(1/M^2)$] by

$$u_h(p) = \left[1 - \frac{i}{2M} \boldsymbol{\gamma} \cdot \mathbf{p} \right] u_Q(p) \quad (7)$$

and where u_Q satisfies $\gamma_0 u_Q(p) = u_Q(p)$.

We now carry out the continuum calculation to the same order for a pseudoscalar current $P = \bar{q}(x)\gamma_5 h(x)$ and obtain

$$\begin{aligned} \langle q(p')|P|h(p)\rangle_{\text{QCD}} &= a_1 \bar{u}_q(p') \gamma_5 u_h(p) \\ &+ a_2 \frac{\mathbf{p} \cdot \mathbf{p}'}{M^2} \bar{u}_q(p') \gamma_5 u_h(p), \end{aligned} \quad (8)$$

where \bar{u}_q and u_h are Dirac spinors and

$$\begin{aligned} a_1 &= 1 + \frac{\alpha_s}{3\pi} \left[\frac{13}{4} + 3 \ln \frac{\mu}{M} + 3 \ln \frac{\mu}{\lambda} \right], \\ a_2 &= \frac{\alpha_s}{3\pi} \left[4 - \frac{8\pi M}{3\lambda} \right]. \end{aligned} \quad (9)$$

Here μ is the scale parameter from dimensional regularization and λ is the gluon mass. We expand the heavy quark energy and Dirac spinor to $1/M$ and obtain

$$\langle q(p')|P|h(p)\rangle_{\text{QCD}} = \eta_P^{(0)}\Omega_P^{(0)} + \eta_P^{(1)}\Omega_P^{(1)} + \eta_P^{(2)}\Omega_P^{(2)} \quad (10)$$

with $\eta_P^{(j)}$ defined in an analogous way to Eq. (4) and

$$\begin{aligned} B_P^{(0)} &= B_{A_0}^{(0)} + \frac{1}{\pi} \left[2 \ln \frac{\mu}{M} + \frac{4}{3} \right], \\ B_P^{(1)} &= B_{A_0}^{(1)} + \frac{1}{\pi} \left[2 \ln \frac{\mu}{M} + \frac{8}{3} \right], \\ B_P^{(2)} &= B_{A_0}^{(2)} - \frac{4}{3\pi}. \end{aligned} \quad (11)$$

Note that $B_P^{(0)}$ and $B_P^{(1)}$ have the same value $[(a_1 - 1)/\alpha_s]$ coming from the first term on the right-hand side of Eq. (8). A check on these results comes from applying the continuum PCAC relation. This shows that the leading order term $B^{(0)}$ should differ between P and A_0 by an amount that is the one-loop conversion factor between the pole and $\overline{\text{MS}}$ quark mass at scale μ . Using $\gamma_0 u_Q = u_Q$ the relationship between the operator matrix elements for the pseudoscalar and temporal axial current cases are

$$\begin{aligned} \Omega_P^{(0)} &= \bar{u}_q(p')\gamma_5 u_Q(p) = \Omega_{A_0}^{(0)}, \\ \Omega_P^{(1)} &= -i\bar{u}_q(p')\gamma_5 \frac{\boldsymbol{\gamma} \cdot \mathbf{P}}{2M} u_Q(p) = -\Omega_{A_0}^{(1)}, \\ \Omega_P^{(2)} &= i\bar{u}_q(p')\frac{\boldsymbol{\gamma} \cdot \mathbf{P}'}{2M}\gamma_0\gamma_5 u_Q(p) = \Omega_{A_0}^{(2)} \end{aligned} \quad (12)$$

with a sign change for the leading relativistic correction, $j = 1$. Exactly the same relations are obtained for the scalar case with respect to the temporal vector calculation.

The current operators needed in the lattice NRQCD calculation are readily identified from the $\Omega^{(j)}$ by replacing spinors with fields and converting momentum factors to derivatives. This gives, for the temporal axial-vector case,

$$\begin{aligned} J_{A_0,\text{lat}}^{(0)} &= \bar{q}(x)\gamma_5\gamma_0 Q(x), \\ J_{A_0,\text{lat}}^{(1)} &= -\frac{1}{2m_b}\bar{q}(x)\gamma_5\gamma_0\boldsymbol{\gamma} \cdot \vec{\nabla} Q(x), \\ J_{A_0,\text{lat}}^{(2)} &= -\frac{1}{2m_b}\bar{q}(x)\boldsymbol{\gamma} \cdot \vec{\nabla}\gamma_0\gamma_5\gamma_0 Q(x), \end{aligned} \quad (13)$$

where m_b is the bare lattice NRQCD quark mass and $Q(x)$ is the two-component NRQCD field (i.e. a four-component field with zero in the lower two components). The analogous expressions for the pseudoscalar case mirror Eq. (12).

The next step is to calculate the mixing matrix for the lattice operators in lattice QCD perturbation theory through one loop. For the A_0 case

$$\langle q(p')|J_{A_0,\text{lat}}^{(j)}|h(p)\rangle = \sum_j Z_{A_0,ij}\Omega_{A_0}^{(j)} \quad (14)$$

with $Z_{A_0,ij}$ written as [16,17]

$$Z_{A_0,ij} = \delta_{ij} + \alpha_s \left\{ \delta_{ij} \left[\frac{Z_q + Z_b}{2} + Z_{m_b}(1 - \delta_{i0}) \right] + \zeta_{ij}^{A_0} \right\}. \quad (15)$$

Z_q is the coefficient of the one-loop term in the wave-function renormalization for massless lattice quarks, here in the HISQ formalism. Similarly, Z_b is the coefficient of the one-loop term in the lattice NRQCD wave-function renormalization and Z_{m_b} the coefficient of the one-loop mass renormalization between the bare NRQCD quark mass and the pole mass [18]. This latter factor appears for $j = 1, 2$ because of the explicit mass factor in the operator and our choice to use the bare NRQCD mass in the NRQCD operators relevant for the lattice calculation. ζ_{ij} are the coefficients of the one-loop terms obtained from the renormalization of the vertex diagram with $J^{(j)}$ at the vertex. Note that Z_b , Z_{m_b} , and ζ_{ij} are all functions of am_b and must be evaluated at the value of am_b being used in the lattice QCD calculation.

Peeling off the external states we can then write, using A_0 as an example,

$$A_0 = \sum_{i,j} \eta_{A_0}^{(i)} Z_{A_0,ij}^{-1} J_{A_0,\text{lat}}^{(j)}, \quad (16)$$

which determines the C_j coefficients of Eq. (2). To make the C_j explicit as a power series in α_s we expand the inverse of Z to $\mathcal{O}(\alpha_s)$,

$$Z_{A_0,ij}^{-1} = \delta_{ij} - \alpha_s \left\{ \delta_{ij} \left[\frac{Z_q + Z_b}{2} + Z_{m_b}(1 - \delta_{i0}) \right] + \zeta_{ij}^{A_0} \right\}. \quad (17)$$

Then, substituting in the results for the $\eta^{(i)}$ from Eq. (4), we have [16]

$$\begin{aligned} C_{0,A_0} &= 1 + \alpha_s \left(B_{A_0}^{(0)} - \frac{Z_q + Z_b}{2} - \zeta_{00}^{A_0} - \zeta_{10}^{A_0} \right), \\ C_{1,A_0} &= 1 + \alpha_s \left(B_{A_0}^{(1)} - \frac{Z_q + Z_b}{2} - Z_{m_b} - \zeta_{11}^{A_0} - \zeta_{01}^{A_0} \right), \\ C_{2,A_0} &= \alpha_s (B_{A_0}^{(2)} - \zeta_{02}^{A_0} - \zeta_{12}^{A_0}). \end{aligned} \quad (18)$$

Z_q and Z_b have logarithmic infrared divergences with $a\lambda$ as do $\zeta_{00}^{A_0}$ and $\zeta_{11}^{A_0}$. These cancel against the logarithmic divergences in $B_{A_0}^{(0)}$ and $B_{A_0}^{(1)}$ [see Eq. (5)] so that C_{0,A_0} and C_{1,A_0} are finite. Similarly the linear infrared divergence of $B_{A_0}^{(2)}$ is canceled by a matching divergence in $\zeta_{02}^{A_0}$. Note that the explicit factors of aM remaining in the $B_{A_0}^{(j)}$ will now be replaced by am_b , which is the same as aM to this

order in α_s . Combinations of the $\zeta_{ij}^{A_0}$ that allow the C_{j,A_0} to be determined are given for the NRQCD-HISQ case in [10], using techniques from [19]. The calculation is done for the standard v^4 -accurate NRQCD action [20,21], but the results are also correct for the $\alpha_s v^4$ -improved NRQCD that we will use here [22], because the impact of the $\alpha_s v^4$ improvement terms will only appear in the matching at α_s^2 .

Here we recast the expansion of the QCD currents into a more natural combination of lattice QCD currents as

$$A_0 = (1 + \alpha_s z_0^{A_0}) \times (J_{A_0,\text{lat}}^{(0)} + (1 + \alpha_s z_1^{A_0}) J_{A_0,\text{lat}}^{(1)} + \alpha_s z_2^{A_0} J_{A_0,\text{lat}}^{(2)}), \quad (19)$$

where, to $\mathcal{O}(\alpha_s)$, $(1 + \alpha_s z_0^{A_0}) = C_{0,A_0}$, $\alpha_s z_2^{A_0} = C_{2,A_0}$ and $\alpha_s z_1^{A_0} = C_{1,A_0} - C_{0,A_0}$. The values for $z_0^{A_0}$, $z_1^{A_0}$, and $z_2^{A_0}$ were given in [9] and are reproduced here in Table II. The values are the same for the temporal vector current from the chiral symmetry of the HISQ action.

To perform the equivalent calculation for the pseudoscalar current we note that the $\Omega_P^{(j)}$ are simply related to the $\Omega_{A_0}^{(j)}$ as in Eq. (12) and so the $J_P^{(j)}$ are similarly related to $J_{A_0}^{(j)}$. Hence we do not need to perform a new calculation in lattice QCD perturbation theory. We simply need to reconstruct the mixing matrix for the pseudoscalar case from that of the temporal axial vector. We can then write

$$P = \sum_j C_{j,P} J_{A_0,\text{lat}}^{(j)} \quad (20)$$

and find

$$\begin{aligned} C_{0,P} &= 1 + \alpha_s \left(B_P^{(0)} - \frac{Z_q + Z_b}{2} - \zeta_{00}^{A_0} + \zeta_{10}^{A_0} \right), \\ C_{1,P} &= -1 - \alpha_s \left(B_P^{(1)} - \frac{Z_q + Z_b}{2} - Z_{m_b} - \zeta_{11}^{A_0} + \zeta_{01}^{A_0} \right), \\ C_{2,P} &= \alpha_s (B_P^{(2)} - \zeta_{02}^{A_0} + \zeta_{12}^{A_0}). \end{aligned} \quad (21)$$

Note the overall minus sign for $C_{1,P}$ as well as the fact that all of the ζ_{ij} factors with either i or j equal to 1 now come in with opposite sign. These factors are all finite, so the $C_{j,P}$ are still manifestly infrared finite.

Table I gives results for the finite ζ factors, $\zeta_{10}^{A_0}$, $\zeta_{01}^{A_0}$, and $\zeta_{12}^{A_0}$, as well as Z_{m_b} that allow us to determine the $C_{j,P}$ from the C_{j,A_0} for a variety of values of the heavy quark mass in lattice units, am_b . These correspond to the values of b quark masses used in our lattice NRQCD calculations that will be discussed in Sec. III.

For the pseudoscalar current case, we multiply both sides of Eq. (20) by the heavy quark mass in the $\overline{\text{MS}}$ scheme at the scale μ and then, on the right-hand side, convert these into lattice NRQCD bare quark masses using the relation

TABLE I. Values for the 3 ζ_{ij} one-loop mixing coefficients [defined in Eq. (15)] needed to determine the renormalization of the lattice NRQCD-HISQ pseudoscalar/scalar current from that of the temporal axial vector/temporal vector current for massless HISQ quarks. Column 5 gives the one-loop NRQCD mass renormalization coefficient. These results were calculated and presented as the linear combination relevant for Eq. (18) in [10] using the standard v^4 -accurate NRQCD action (with stability parameter $n = 4$) and the individual values are given here. We also include new results for a lighter b quark mass, $am_b = 1.22$, suitable for the MILC ‘‘superfine’’ (0.06 fm) lattices.

| am_b | $\zeta_{10}^{A_0}$ | $\zeta_{01}^{A_0}$ | $\zeta_{12}^{A_0}$ | Z_{m_b} |
|--------|--------------------|--------------------|--------------------|-----------|
| 3.297 | -0.0958(1) | -0.1918(1) | 0.029(4) | 0.167(1) |
| 3.263 | -0.0966(1) | -0.1941(1) | 0.030(4) | 0.176(1) |
| 3.250 | -0.0970(1) | -0.1950(1) | 0.031(4) | 0.178(1) |
| 2.688 | -0.1144(1) | -0.2379(1) | 0.060(4) | 0.262(1) |
| 2.660 | -0.1156(1) | -0.2411(1) | 0.060(4) | 0.264(1) |
| 2.650 | -0.1157(1) | -0.2414(1) | 0.061(4) | 0.267(1) |
| 2.620 | -0.1171(1) | -0.2448(1) | 0.062(4) | 0.272(1) |
| 1.910 | -0.1539(1) | -0.3256(1) | 0.093(4) | 0.434(1) |
| 1.890 | -0.1553(1) | -0.3285(1) | 0.095(4) | 0.448(1) |
| 1.832 | -0.1593(2) | -0.3361(1) | 0.097(4) | 0.466(1) |
| 1.826 | -0.1595(2) | -0.3370(1) | 0.098(4) | 0.468(1) |
| 1.220 | -0.2258(5) | -0.4625(5) | 0.116(5) | 0.714(1) |

$$m_b^{\overline{\text{MS}}}(\mu) = m_b \left[1 + \alpha_s \left(Z_{m_b} - \frac{2}{\pi} \ln \frac{\mu}{M} - \frac{4}{3\pi} \right) \right]. \quad (22)$$

Values for Z_{m_b} at a variety of am_b values for lattice NRQCD are given in Table I [10]. Then we have

$$\begin{aligned} P(\mu) m_b^{\overline{\text{MS}}}(\mu) &= m_b (1 + \alpha_s z_0^P) \\ &\times (J_{A_0,\text{lat}}^{(0)} - (1 + \alpha_s z_1^P) J_{A_0,\text{lat}}^{(1)} + \alpha_s z_2^P J_{A_0,\text{lat}}^{(2)}). \end{aligned} \quad (23)$$

TABLE II. Values for the one-loop renormalization factors for the NRQCD-HISQ temporal axial vector current [defined in Eq. (19)] for massless HISQ quarks. The results for the temporal vector current are identical. These were calculated in [9] from numbers in [10] and are reproduced here. The results for $z_2^{A_0}$ have changed slightly for the heaviest masses because of an improved calculation of ζ_{02} .

| am_b | $z_0^{A_0}$ | $z_1^{A_0}$ | $z_2^{A_0}$ |
|--------|-------------|-------------|-------------|
| 3.297 | 0.0238(20) | 0.0242(28) | -1.014(6) |
| 3.263 | 0.0216(20) | 0.0244(28) | -1.009(6) |
| 3.250 | 0.0220(10) | 0.0240(22) | -0.999(6) |
| 2.688 | 0.0054(20) | 0.0076(28) | -0.712(4) |
| 2.660 | 0.0056(20) | 0.0074(28) | -0.698(4) |
| 2.650 | 0.0037(20) | 0.0093(28) | -0.696(4) |
| 2.620 | 0.0011(20) | 0.0069(28) | -0.690(4) |
| 1.910 | -0.0071(20) | -0.0309(36) | -0.325(4) |
| 1.890 | -0.0067(20) | -0.0313(36) | -0.318(4) |
| 1.832 | -0.0027(20) | -0.0393(36) | -0.314(4) |
| 1.826 | -0.0035(30) | -0.0395(42) | -0.311(4) |
| 1.220 | 0.0658(40) | -0.0834(58) | 0.027(9) |

TABLE III. The results from this paper are the values for the one-loop renormalization factors for the NRQCD-HISQ pseudoscalar current [defined in Eq. (23)] for massless HISQ quarks. Results for the scalar current are identical.

| am_b | z_0^P | z_1^P | z_2^P |
|--------|-------------|-------------|------------|
| 3.297 | -0.0008(22) | 0.2566(28) | -1.380(10) |
| 3.263 | 0.0044(22) | 0.2538(28) | -1.373(10) |
| 3.250 | 0.0060(14) | 0.2524(22) | -1.361(10) |
| 2.688 | 0.0386(22) | 0.1850(28) | -1.016(9) |
| 2.660 | 0.0384(22) | 0.1808(28) | -1.002(9) |
| 2.650 | 0.0393(22) | 0.1823(28) | -0.998(9) |
| 2.620 | 0.0389(22) | 0.1759(28) | -0.990(9) |
| 1.910 | 0.1191(22) | 0.0501(36) | -0.563(9) |
| 1.890 | 0.1307(22) | 0.0467(36) | -0.552(9) |
| 1.832 | 0.1447(22) | 0.0315(36) | -0.544(9) |
| 1.826 | 0.1455(32) | 0.0299(43) | -0.539(9) |
| 1.220 | 0.3278(40) | -0.1324(59) | -0.165(14) |

We find

$$\begin{aligned}
 z_0^P &= z_0^{A_0} + 2\zeta_{10}^{A_0} + Z_{m_b}, \\
 z_1^P &= z_1^{A_0} + 2\zeta_{01}^{A_0} - 2\zeta_{10}^{A_0} + \frac{4}{3\pi}, \\
 z_2^P &= z_2^{A_0} + 2\zeta_{12}^{A_0} - \frac{4}{3\pi}.
 \end{aligned} \tag{24}$$

The values of appropriate ζ_{ij} and Z_{m_b} given in Table I enable us to determine the z_j^P values from the $z_j^{A_0}$. The z_j^P values are given in Table III. The values are the same for the scalar current due to the chiral symmetry of the HISQ action.

Figure 2 shows the different contributions to $z_0^{A_0}$ and z_0^P as a function of am_b . This includes the finite pieces of each of the terms in Eq. (21) that vary with am_b (thereby excluding Z_q). The different contributions are all of moderate size and show mild dependence on am_b over the range of am_b values that we use.

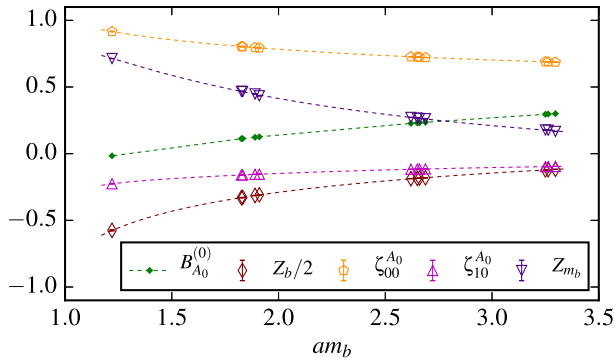


FIG. 2. The different contributions that make up the renormalization coefficients $z_0^{A_0}$ and z_0^P as a function of the bare heavy quark mass in the lattice NRQCD Hamiltonian, as given in Eqs. (21) and (24). The infrared-finite pieces are plotted for infrared-divergent contributions, and Z_q is not included since it does not vary with am_b .

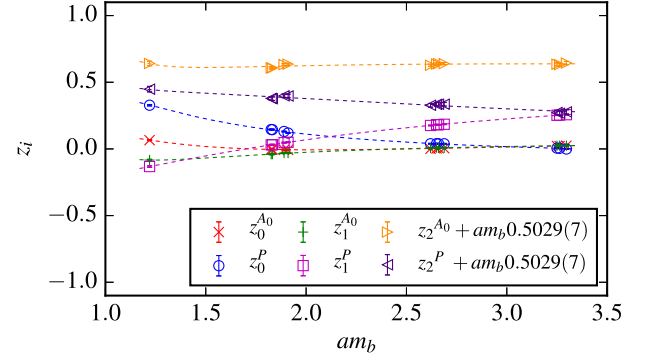


FIG. 3. The z_0 and z_1 factors for the $\mathcal{O}(\alpha_s)$ matching of the temporal axial and pseudoscalar NRQCD-HISQ currents to continuum QCD [Eqs. (19) and (23)] plotted against the bare lattice b -quark mass.

In Fig. 3 we plot z_0 and z_1 for the temporal axial vector and pseudoscalar cases. The magnitudes of $z_0^{A_0}$ and $z_1^{A_0}$ are both very small and both have very little dependence on am_b , a fact previously remarked on in [9]. z_0^P and z_1^P have larger magnitude and somewhat more dependence on am_b . However, both are still smaller than 1 across the range of am_b values we use.

Note that using $J^{(0)}$ alone in NRQCD to approximate either the temporal axial vector or pseudoscalar currents gives a larger renormalization factor at $\mathcal{O}(\alpha_s)$. This is because the coefficient that represents the “mixing-down” of $J^{(1)}$ into $J^{(0)}$, ζ_{10} , reduces the size of the one-loop renormalization of the combined current in both cases. That $J^{(0)} + J^{(1)}$ is much closer to the continuum current than $J^{(0)}$ will be demonstrated in an order-by-order comparison of results in Sec. III.

The coefficients $z_2^{A_0}$ and z_2^P have stronger am_b dependence dominated by that in the mixing coefficient ζ_{02} . This grows linearly with am_b at large values of am_b so that, as $am_b \rightarrow \infty$, the contribution of $J^{(2)}$ becomes an $\alpha_s a \Lambda_{\text{QCD}}$ correction term. In Fig. 4 we show ζ_{02}/am_b up to large values of am_b (much above those that we use in practice)

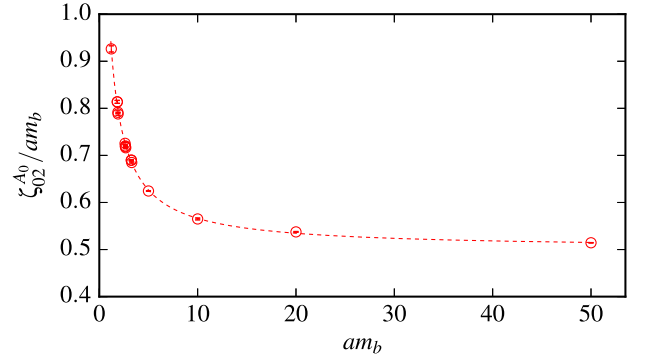


FIG. 4. The one-loop mixing coefficient $\zeta_{02}^{A_0}$ for the temporal axial vector NRQCD-HISQ current for massless HISQ quarks divided by the bare heavy quark mass, am_b , and plotted against am_b . This shows that ζ_{02} grows linearly with am_b as $am_b \rightarrow \infty$.

TABLE IV. Sets of MILC configurations [23,24] used here with their (HISQ) sea quark masses, $m_l [= (m_u + m_d)/2]$, m_s , and m_c in lattice units. $\beta = 10/g^2$ is the QCD gauge coupling and the lattice spacing, a , is determined using the $\Upsilon(2S - 1S)$ splitting [9,22]. The lattice size is $L_s^3 \times L_t$. Each ensemble contains around 1000 configurations, and we take 16 time sources per configuration to increase statistics.

| Set | β | a [fm] | am_l^{sea} | am_s^{sea} | am_c^{sea} | am_s^{val} | am_b^{val} | L_s/a | L_t/a |
|-----|---------|------------------|---------------------|---------------------|---------------------|---------------------|---------------------|---------|---------|
| 1 | 5.80 | 0.1474(5)(14)(2) | 0.013 | 0.065 | 0.838 | 0.0641 | 3.297 | 16 | 48 |
| 2 | 5.80 | 0.1463(3)(14)(2) | 0.0064 | 0.064 | 0.828 | 0.0636 | 3.263 | 24 | 48 |
| 3 | 5.80 | 0.1450(3)(14)(2) | 0.00235 | 0.0647 | 0.831 | 0.0628 | 3.25 | 32 | 48 |
| 4 | 6.00 | 0.1219(2)(9)(2) | 0.0102 | 0.0509 | 0.635 | 0.0522 | 2.66 | 24 | 64 |
| 5 | 6.00 | 0.1195(3)(9)(2) | 0.00507 | 0.0507 | 0.628 | 0.0505 | 2.62 | 32 | 64 |
| 6 | 6.00 | 0.1189(2)(9)(2) | 0.00184 | 0.0507 | 0.628 | 0.0507 | 2.62 | 48 | 64 |
| 7 | 6.30 | 0.0884(3)(5)(1) | 0.0074 | 0.0370 | 0.440 | 0.0364 | 1.91 | 32 | 96 |
| 8 | 6.30 | 0.0873(2)(5)(1) | 0.0012 | 0.0363 | 0.432 | 0.0360 | 1.89 | 64 | 96 |

where this behavior becomes clear. At the am_b values that we use, the $\alpha_s a \Lambda_{\text{QCD}}$ and $\alpha_s \Lambda_{\text{QCD}}/m_b$ behavior is intertwined. Values of $z_2^{A_0}$ and z_2^P with the linear am_b term removed are shown in Fig. 3.

Lattice QCD results can be combined with Eqs. (19) and (23) to determine the hadronic matrix elements of the temporal axial vector/vector and pseudoscalar/scalar currents up to systematic uncertainties coming from missing higher order radiative and relativistic corrections (which will differ between the currents). In Sec. III we will compare results for hadronic decay constants obtained using temporal axial or pseudoscalar currents and form factors from temporal vector and scalar currents. The extent to which they agree is a test of our systematic uncertainties.

III. LATTICE CALCULATION AND RESULTS

A. Lattice configurations and simulation parameters

The gluon field configurations used here are listed in Table IV. They are “second-generation” MILC configurations [23,24] using a gluon action fully corrected through $\alpha_s a^2$ [25] and HISQ quarks [8] with u , d , s , and c ($n_f = 2 + 1 + 1$) flavors in the sea. They include multiple values of the lattice spacing and multiple values of the u/d (taken to be degenerate) sea quark mass varying from one-fifth of the s quark mass down to the physical value. On these gluon field configurations the B and B_s decay constants were calculated in [9] using a radiatively improved (through $\alpha_s v_b^4$) NRQCD action for the b quark [22,26], the HISQ action for the lighter quark, and an NRQCD-HISQ temporal axial current matched to continuum QCD following the process described in Sec. II. Here we will compare results using the pseudoscalar current matched to the same level of accuracy. In a similar way, the systematic uncertainties in the semileptonic form factor for $B \rightarrow \pi$ obtained from (the traditional method of) using a vector current can be tested by employing a scalar current. Since we are largely reusing results from earlier papers [9,27], we do not repeat technical details, for example on the NRQCD Hamiltonian, but refer the reader to those papers for more detail.

B. B and B_s meson decay constants

Using the PCAC relation of continuum QCD we can determine the B meson decay constant, f_B , from the matrix element of the temporal axial current between the vacuum and a B meson (at rest) as

$$\langle 0 | A_0 | B \rangle = f_B M_B \quad (25)$$

or from the product of the pseudoscalar density and the quark masses as

$$(m_b + m_l) \langle 0 | P | B \rangle = f_B M_B^2. \quad (26)$$

Here M_B is the B meson mass. In [9] the temporal axial current relationship of Eq. (25) was used. A_0 was constructed from the leading and next-to-leading NRQCD-HISQ currents in a nonrelativistic expansion and was matched to continuum QCD according to Eq. (19). This involves writing A_0 in terms of the lattice currents, $J_{A_0,\text{lat}}^{(0)}$, $J_{A_0,\text{lat}}^{(1)}$, and $J_{A_0,\text{lat}}^{(2)}$. In [9] the matrix elements of each current between the vacuum and a B meson are determined in lattice QCD, so that the matrix element of A_0 in Eq. (25) can be obtained to the specified level of accuracy (the matrix elements for $J_{A_0,\text{lat}}^{(1)}$ and $J_{A_0,\text{lat}}^{(2)}$ are the same for a meson at rest). Since $J^{(1)}$ and $J^{(2)}$ are relativistic corrections to $J^{(0)}$, we expect their matrix elements to be of relative size Λ_{QCD}/m_b ($\approx 10\%$) compared to that of $J^{(0)}$ for a B meson at rest, where internal momenta are of $\mathcal{O}(\Lambda_{\text{QCD}})$.¹ Terms in which $J^{(1)}$ and $J^{(2)}$ matrix elements are multiplied by α_s might then be expected to be of relative size $\alpha_s \times 10\% \approx 3\%$.

In Eq. (23) we give an expansion to the same order for the combination of quark mass and pseudoscalar density, $m_b P$, in terms of the same NRQCD-HISQ currents

¹Because of the mixing-down effects discussed in Sec. II, part of the $J^{(1)}$ and $J^{(2)}$ matrix elements is proportional to α_s times the matrix element of $J^{(0)}$. This is a small effect here because the relevant coefficient, ζ_{10} , is small (see Fig. 2).

multiplied by the bare NRQCD quark mass. Because the matrix elements for each of the lattice NRQCD-HISQ currents are given in [9], we can reconstruct the matrix element of $m_b P$ required on the left-hand side of Eq. (26) and so determine the decay constant in a different way. This decay constant should agree with that determined from the temporal axial current up to the uncertainties quoted. These are dominated by systematic errors from missing higher order matching terms and relativistic current corrections [9].

Figure 5 shows how well this process works order-by-order as relativistic current corrections and α_s matching terms are added in. The variations match our power-counting expectations well, as we discuss further below. The plot shows the ratio of the decay constant obtained using the temporal axial current to that using the

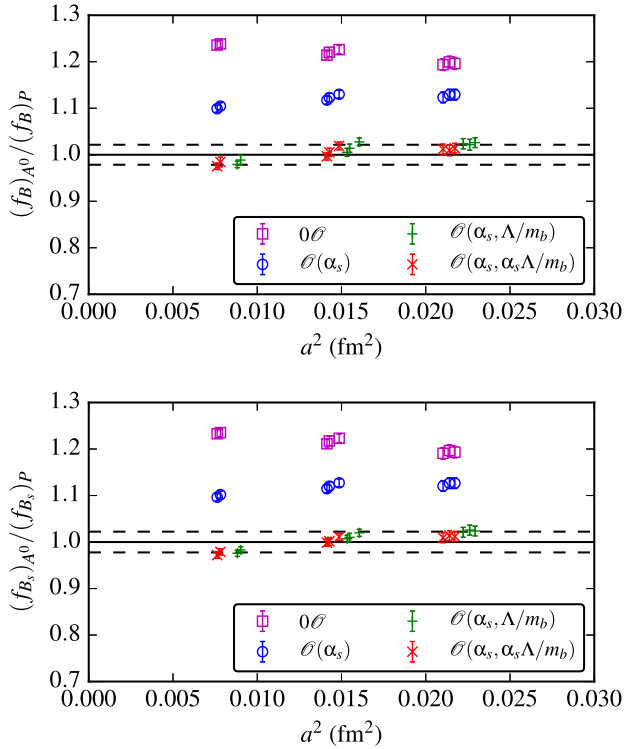


FIG. 5. The ratio of the decay constant obtained using the temporal axial current to that obtained using the pseudoscalar density. Results are from lattice QCD calculations of the matrix element from a nonrelativistic expansion of the appropriate current operator between the vacuum and a B meson (upper plot) or B_s meson (lower plot). Results from each of the ensembles of Table IV are shown plotted against the square of the lattice spacing. Purple open squares denote the lowest (zeroth) order result, while blue open circles include only $J_{A_0, \text{lat}}^{(0)}$ but with $\mathcal{O}(\alpha_s)$ matching for that current. Green pluses include $J_{A_0, \text{lat}}^{(1)}$ in a matching through $\mathcal{O}(\alpha_s)$ and red crosses include the full matching of Eqs. (19) and (23). Green pluses have been offset for clarity. The dashed lines show the relative uncertainty on f_B values quoted in [9].

pseudoscalar density. We use the results from [9], which gives matrix elements for each contribution to the current on each of the ensembles in Table IV. For each ensemble the bare NRQCD quark mass am_b is tuned to that of the b quark using the spin average of Υ and η_b masses, and the u/d quark mass, am_l , is given the value used for the light quark mass in the sea. The s quark mass is tuned using a fictitious $s\bar{s}$ pseudoscalar meson whose properties are well determined in lattice QCD [28]. Values for the π , K , and η_s meson masses made from these light quarks are given in [28,29]. We use α_s in the V-scheme at a scale $2/a$ in the operator matching as in [9].

In the determination of f_B from the pseudoscalar density in Eq. (26) there is a factor of $(1 + m_l/m_b)$ on the left-hand side. We neglect this for the u/d quark because, at the physical point, $m_l/m_b = 1/(52.55 \times 27.4)$ [30]. This is negligible compared to the other uncertainties. For the additional factor of m_B on the right-hand side, which must be removed to take a ratio of the two different decay constants, we use the average of the charged and neutral experimental B meson masses [1]. It has already been demonstrated that the lattice QCD result for the B meson mass, using NRQCD for the b quark, agrees with experiment at the physical value of the u/d quark mass [29].

In the upper plot of Fig. 5 (for the B meson) the lowest (zeroth) order result includes only the $J_{A_0, \text{lat}}^{(0)}$ current at tree level, whose matrix element cancels in the ratio, and so the result is simply m_b/M_B . Not surprisingly, substantial differences are seen between the results of $\mathcal{O}(20\%)$, being the size of the binding energy of a B meson. A significant improvement is seen on including α_s radiative corrections to the normalization of $J_{A_0, \text{lat}}^{(0)}$ in the open blue circles. Note that, as remarked in Sec. II, the renormalization of $J_{A_0, \text{lat}}^{(0)}$ differs from that of $J_{A_0, \text{lat}}^{(0)} + J_{A_0, \text{lat}}^{(1)}$ because of mixing-down effects encapsulated in $\zeta_{10}^{A_0}$. The differences between the two decay constants are now $\mathcal{O}(10\%)$ reflecting missing relativistic corrections of $\mathcal{O}(\Lambda_{\text{QCD}}/m_b)$. The green pluses and red crosses now successively include the effect of $J_{A_0, \text{lat}}^{(1)}$ at tree level and then α_s corrections multiplying the matrix elements of both $J_{A_0, \text{lat}}^{(1)}$ and $J_{A_0, \text{lat}}^{(2)}$ (which are the same here). The green pluses and red crosses are very close together, since the final α_s corrections have little impact.

The final result, correct through $\alpha_s \Lambda_{\text{QCD}}/m_b$, denoted by the red crosses in Fig. 5 is close to the solid line at 1.0, which indicates the same result is obtained for the decay constant from both the temporal axial current and pseudoscalar density. More importantly the differences from the value 1.0 of this ratio lie within the dashed lines that correspond to the 2.2% relative uncertainty quoted for f_B from the temporal axial current in [9]. This uncertainty was dominated by an estimate of the uncertainties expected from missing higher order relativistic current corrections

and α_s^2 matching errors. Since the results from the temporal axial current and pseudoscalar density will have different uncertainties from the missing α_s^2 matching, the result of Fig. 5 is a demonstration that the estimates of these uncertainties are realistic.

The lower plot of Fig. 5 repeats this exercise for the decay constant of the B_s meson, again using results from [9]. In this case, using Eq. (26), we do not neglect the s quark mass on the left-hand side. Instead we write

$$\left(1 + \frac{m_s}{m_b}\right) m_b \langle 0 | P | B_s \rangle = f_{B_s} M_{B_s}^2, \quad (27)$$

and take $m_s/m_b = 1.0/52.55(55)$ [30]. We use the experimental value of the B_s meson mass to determine a ratio of the decay constants from temporal axial current and pseudoscalar density. The lower plot of Fig. 5 has identical features to that of the upper plot. This is not surprising because the relative effect of the matrix elements of the relativistic current corrections is the same for u/d and s quarks as can be seen from the results in [9].

We can complete the analysis by fitting the decay constant results for f_B and f_{B_s} , obtained from the pseudoscalar density, as a function of u/d quark mass and lattice spacing, to extract physical results for comparison to the final answers obtained using the temporal axial current. In the temporal axial current case, because of a normalization factor from the meson states, the hadronic quantity naturally obtained from the lattice QCD calculation is $f_B \sqrt{M_B}$, denoted by Φ . The contributions to Φ from $J_{A_0, \text{lat}}^{(0)}$ and $J_{A_0, \text{lat}}^{(1)}$ are tabulated in [9]. The equivalent hadronic quantity corresponding to matrix elements of $m_b P$ is $f_B (M_B)^{3/2}$. The values we need for $m_b P$ matrix elements are obtained by combining the appropriate Φ values for $J^{(0)}$ and $J^{(1)}$ as in Eq. (23), including multiplication by am_b and then by an additional power of $1/a$ to convert to GeV units. In this case, the additional multiplication by $1/a$ will slightly increase the uncertainty in the values we are fitting because of the uncertainty in the determination of the lattice spacing.

We plot $f_B(\sqrt{M_B})^3$ for the B and B_s mesons in Fig. 6, as well as plot our fits to the light quark mass and lattice spacing dependence that enables us to extract a physical result. Figure 7 shows a similar plot for the ratio for B_s to B . Following [9] we use a fit form

$$\begin{aligned} f_B(\sqrt{M_B})^3(a, M_\pi) &= f_B(\sqrt{M_B})^3(1 + d_1(\Lambda a)^2 + d_2(\Lambda a)^4) \\ &\times \left(1 + b_{1,l} \frac{M_\pi^2}{\Lambda_\chi^2} - \frac{3(1 + 3g^2)}{4\Lambda_\chi^2} l(M_\pi^2)\right) \\ &\times (1 + e_1 \alpha_s^2 [1 + e_2 \delta m_b + e_3 \delta m_b^2]). \end{aligned} \quad (28)$$

Here d_1 and d_2 allow for discretization effects and are also δm_b dependent (suppressed for clarity). b_1 allows for

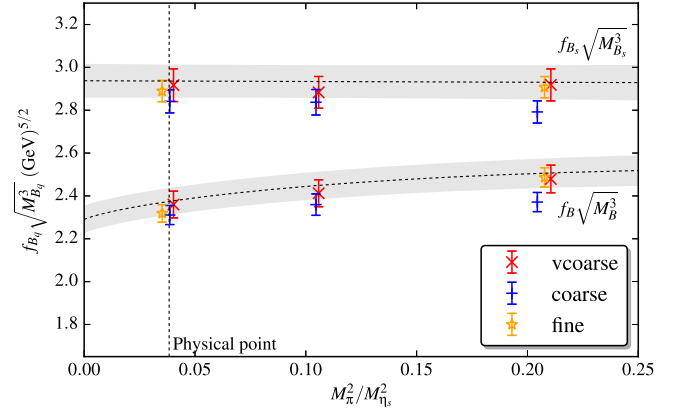


FIG. 6. Results for the decay constants of B and B_s mesons (multiplied by the $3/2$ power of the meson mass) for the ensembles in Table IV, obtained from the pseudoscalar current and plotted against the light quark mass in units of the strange quark mass (given as M_π^2/M_η^2). The grey bands show the results of the fit described in the text. Errors on the data points include statistics/fitting only; the grey band includes the full error from the fit to lattice spacing and quark mass effects along with the perturbative matching uncertainty.

dependence on the light quark mass, including the chiral logarithm, $l(M_\pi^2)$. For the B_s case the chiral logarithm term is not present and $b_{1,l} \rightarrow b_{1,s}$. e_1 allows for α_s^2 corrections from only matching to one loop in perturbation theory, while $e_{2,3}$ allow for the fact that the higher order matching coefficients can in principle have am_b dependence. These priors are given identical values as in [9], except for $e_1 = 0.0(3)$ as the pseudoscalar matching coefficients are slightly larger than their temporal axial-vector counterparts. Extrapolating to the physical point in the absence of electromagnetism, i.e. $M_\pi = M_{\pi_0}$, where $m_l = (m_u + m_d)/2$, we find $f_B(M_B)^{3/2} = 2.37(7) \text{ GeV}^{3/2}$, $f_{B_s}(M_{B_s})^{3/2} = 2.94(8) \text{ GeV}^{3/2}$, and $f_{B_s}(M_{B_s})^{3/2}/f_B(M_B)^{3/2} = 1.237(7)$.

Our complete error budget is given in Table V, with a breakdown that follows [9]. Errors arising from statistics, the lattice spacing, operator matching, and chiral parameters are estimated directly from the fit. The remaining source of systematic error in the decay constants comes from missing higher order relativistic corrections to the

TABLE V. Full error budget for $f_{B_s}(M_{B_s})^{3/2}$, $f_B(M_B)^{3/2}$, and their ratio as a percentage of the final answer.

| Error % | Ratio | $f_{B_s}(M_{B_s})^{3/2}$ | $f_B(M_B)^{3/2}$ |
|----------------|-------|--------------------------|------------------|
| a dependence | 0.0 | 1.1 | 1.1 |
| Chiral | 0.02 | 0.12 | 0.13 |
| g | 0.0 | 0.01 | 0.01 |
| Stat/scale | 0.3 | 1.1 | 1.1 |
| Operator | 0.0 | 2.0 | 2.1 |
| Relativistic | 0.5 | 1.0 | 1.0 |
| Total | 0.6 | 2.8 | 2.8 |

current. As discussed in [9], for the heavy-light system under consideration the higher order relativistic corrections will be of the size $(\Lambda_{\text{QCD}}/am_b)^2 \simeq 0.01$, which we take for this component of the error.

We can convert the above results into values of the decay constants using the PDG masses [31] for $M_{B_i} = (M_{B_0} + M_{B^\pm})/2 = 5.27963(15)$ GeV and $M_{B_s} = 5.36689(19)$. Our final results for the decay constants obtained from the pseudoscalar current are $f_B = 0.196(6)$ GeV, $f_{B_s} = 0.236(7)$ GeV, and $f_{B_s}/f_B = 1.207(7)$.

As the same matrix elements are used as input when determining the decay constant from temporal axial-vector and pseudoscalar currents, we must include correlations when performing an average of the results obtained here and in [9]. As the different values for $f_{B_{(s)}}$ are slightly outside the 1σ error, we scale the error of the weighted averaged value by $\sqrt{\chi^2/\text{d.o.f.}}$ when the $\chi^2/\text{d.o.f.} \geq 1$. This is a conservative option and gives the scaled weighted averages as $f_B = 0.190(4)$ GeV, $f_{B_s} = 0.229(5)$ GeV, and $f_{B_s}/f_B = 1.206(5)$. These are shown and compared to previous determinations, in Fig. 10, to be discussed further in Sec. IV.

C. Scalar form factor for $B \rightarrow \pi$ decay

Another process where accurate determination of the matrix elements of heavy-light currents is required is for the weak semileptonic decays of B mesons to light mesons. The archetypal process here is $B \rightarrow \pi \ell \nu$. The hadronic parameters needed to determine the rate for this decay are known as form factors, and they are now functions of q^2 , the squared 4-momentum transfer between the initial and final mesons. For $B \rightarrow \pi \ell \nu$ there are two form factors which we will denote f_+ and f_0 , but the experimental rate is sensitive to f_+ (only) if the final state lepton is light. The form factors are related to the matrix elements of vector and scalar currents by

$$\begin{aligned} \langle \pi | V^\mu | B \rangle &= f_+(q^2) \left[p_B^\mu + p_\pi^\mu - \frac{M_B^2 - M_\pi^2}{q^2} q^\mu \right] \\ &+ f_0(q^2) \frac{M_B^2 - M_\pi^2}{q^2} q^\mu \end{aligned} \quad (29)$$

and

$$\langle \pi | S | B \rangle = f_0(q^2) \frac{M_B^2 - M_\pi^2}{m_b - m_l}. \quad (30)$$

There is a kinematic constraint that $f_+(0) = f_0(0)$.

At the zero recoil, maximum q^2 , point we can compare the matrix elements of the temporal vector and scalar currents directly. At that point, where $q^0 = M_B - M_\pi$,

$$\langle \pi | V^0 | B \rangle = f_0(q_{\text{max}}^2)(M_B + M_\pi) \quad (31)$$

and

$$\frac{m_b - m_l}{M_B - M_\pi} \langle \pi | S | B \rangle = f_0(q_{\text{max}}^2)(M_B + M_\pi). \quad (32)$$

For currents made of NRQCD b quarks combined with HISQ light quarks, the chiral symmetry of the HISQ action guarantees that the nonrelativistic expansion of the temporal vector current has the same form as for the temporal axial vector current given in Eq. (19). Likewise $m_b S$ has the same expansion as $m_b P$ given in Eq. (23). As for the case of the decay constant discussed in Sec. III B, the currents that appear in each order of the nonrelativistic expansion are the same for S and V^0 . Thus we can construct the matrix element of $m_b S$ given the lattice matrix elements of the different current contributions for V^0 . These are given for the zero recoil situation in [27] for the same $2+1+1$ gluon field configurations as used for the decay constants in Sec. III B, and listed in Table IV.

Figure 8 shows the ratio of the scalar form factor at zero recoil determined from Eqs. (31) and (32) using successively more accurate representations of the NRQCD-HISQ temporal vector and scalar currents from Eqs. (19) and (23). The matrix elements for the individual lattice current pieces are calculated in [27], noting that the matrix element of $J_{V^0}^{(2)}$ is equal to that of $J_{V^0}^{(1)}$ at zero recoil. In the additional mass factors on the left-hand side of Eq. (32) we ignore m_l compared to m_b as it is less than a 0.5% effect across our range of light quark mass values. For M_B we average the charged and neutral B meson masses, as in Sec. III B, and for M_π we use the values appropriate to these ensembles given in [9,29].

Figure 8 shows a very similar picture to that of Fig. 5 with the ratio of the two results becoming closer to 1.0 as

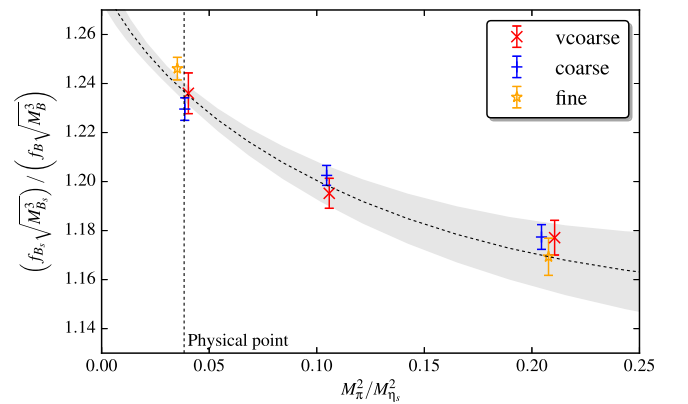


FIG. 7. Results for the ratio of B_s to B decay constants (multiplied by the $3/2$ power of the ratio of meson mass) obtained from the pseudoscalar current. The data points are as shown in Fig. 6, and the grey band is the result of the fit described in the text, including uncertainties from lattice spacing and quark mass effects along with uncertainties from higher-order relativistic corrections to the current.

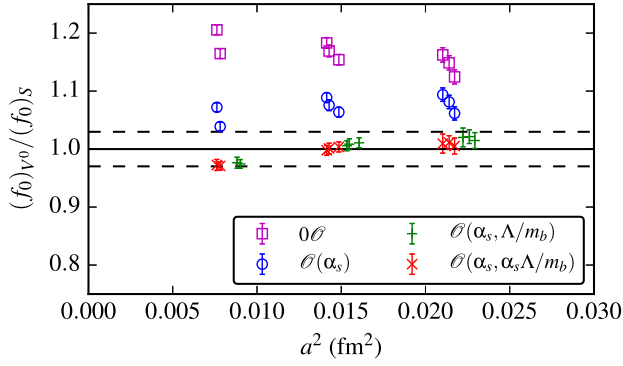


FIG. 8. The ratio of the scalar form factor at zero recoil for the B to π decay obtained from the temporal vector current to that from using the scalar current. Results are from lattice QCD calculations of the matrix element of a nonrelativistic expansion of the appropriate current operator between a π meson and a B meson. Results from each of the ensembles of Table IV are shown plotted against the square of the lattice spacing. Symbols are as in Fig. 5, with the green pluses offset for clarity. The dashed line gives the relative error on $f_0(q_{\max}^2)$ quoted in [27].

nonrelativistic current corrections are included and radiative corrections to them are added. In the case given here, in which the π meson is at rest, the power-counting expectations as higher order currents are added in are the same as for the B meson decay constant case discussed in Sec. III B. Not surprisingly the results mirror the B decay constant case. With the most accurate matching that we have, the ratio of the results for the scalar form factor differs from one by less than the relative uncertainty on $f_0(q_{\max}^2)$ of 3% quoted in [27].

In [27] the ratio of $f_0(q_{\max}^2)$ to the decay constant ratio f_B/f_π was calculated to see if this ratio became one in the massless π meson limit, as expected from soft pion theorems [32–35]. This was indeed found to be the case, resolving a long-standing issue in the literature. The quantity calculated in [27] was

$$R_{B\pi} = \frac{f_0(q_{\max}^2)(1 + M_\pi/M_B)}{[f_B/f_\pi]}, \quad (33)$$

which becomes $f_0(q_{\max}^2)f_\pi/f_B$ as $M_\pi \rightarrow 0$. The piece of this ratio that involves b quarks is $f_0(q_{\max}^2)/f_B$, and this was determined for NRQCD b quarks from the ratio of the matrix element between π and B of the temporal vector current divided by the matrix element between the vacuum and B of the temporal axial vector current. Because of the chiral symmetry of HISQ quarks the matching of these two NRQCD-HISQ currents to their continuum counterparts is the same. Then the overall renormalization factor $(1 + \alpha_s z_0 + \dots)$ [see Eq. (19)] cancels between them, and the renormalization uncertainty from missing α_s^2 and higher order terms is much reduced. The ratio $R_{B\pi}$ can then be determined to high accuracy. In [27] $R_{B\pi}$ was mapped out

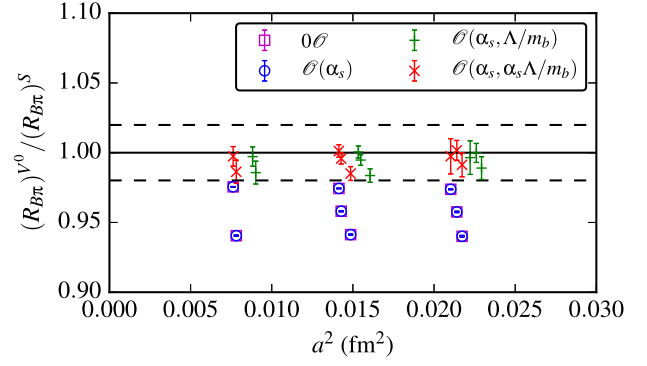


FIG. 9. The ratio of $R_{B\pi}$ values (see text for definition) obtained using a combination of temporal vector and temporal axial vector currents to that from a combination of scalar and pseudoscalar currents. Results from each of the ensembles of Table IV are shown plotted against the square of the lattice spacing. Symbols are as in Fig. 5, with the green pluses offset for clarity. The dashed line gives the relative error on $R_{B\pi}$ from using the temporal vector current for f_0 and temporal axial current for f_B quoted in [27].

as a function of M_π and extrapolated to $M_\pi = 0$ using chiral perturbation theory to show that $R_{B\pi}(M_\pi = 0)$ was close to 1 with an uncertainty of 5%. The temporal vector current was used for $f_0(q_{\max}^2)$ and the temporal axial current for f_B .

Here we can also calculate $R_{B\pi}$, using the scalar current for $f_0(q_{\max}^2)$ and the pseudoscalar current for f_B . Again the overall renormalization factor between the two will cancel [see Eq. (23)]. Figure 9 shows the ratio of $R_{B\pi}$ calculated in these two different ways as, once again, successively more accurate representations of the b -light currents are used. Now, because of cancellation of the overall renormalization factors, there is no difference between the zeroth order result and the $\mathcal{O}(\alpha_s)$ result. Once $\alpha_s \Lambda_{\text{QCD}}/m_b$ corrections are included, the ratio of $R_{B\pi}$ values is very close to one and well within the uncertainty of 2% on $R_{B\pi}(M_\pi = M_{\pi,\text{expt}})$ quoted in [27].

IV. CONCLUSIONS

Here we have given the matching calculation that enables matrix elements of heavy-light scalar and pseudoscalar currents accurate through $\mathcal{O}(\alpha_s \Lambda_{\text{QCD}}/m_b)$ to be determined in lattice QCD using NRQCD b quarks and HISQ light quarks. This expands the range of methods we can apply to B physics using NRQCD and the tests we can do of our systematic error budget.

In Sec. III B we determined the B and B_s meson decay constants using the pseudoscalar current and then compared to the previously determined values obtained from using the temporal axial current [9]. Since there is no PCAC relation connecting these two currents in lattice NRQCD, they do not have to give the same answer. The way in which the nonrelativistic approximation to the continuum current is built up (albeit from the same ingredients) and the way in which it is renormalized are both different in the two cases.

The systematic uncertainties from missing higher order terms will then also be different. We see in Fig. 5 the results coming closer together as we include higher orders in the nonrelativistic expansion and matching on both sides. The final results, at the best accuracy that we can currently achieve, agree to within the expected remaining systematic uncertainty. This uncertainty is dominated by unknown α_s^2 terms in the overall renormalization (multiplying the leading current). The agreement is confirmation that the error budget is a reasonable one. Our results for the B and B_s decay constants from the pseudoscalar current are

$$\begin{aligned} f_B &= 0.196(6) \text{ GeV}, \\ f_{B_s} &= 0.236(7) \text{ GeV}, \\ f_{B_s}/f_B &= 1.207(7). \end{aligned} \quad (34)$$

Our new results for the B and B_s decay constants (and their ratio) can be considered as independent values from those obtained using the temporal axial current in [9]. They use the same raw lattice data in the form of matrix elements for the current components, and so their statistical uncertainties are correlated. Their systematic uncertainties are not the same, however, since they come largely from unknown, and different, relativistic and α_s^2 matching corrections. We can then perform a weighted average of the results arising from the two methodologies, including the statistical correlations, to obtain

$$\begin{aligned} f_B &= 0.190(4) \text{ GeV}, \\ f_{B_s} &= 0.229(5) \text{ GeV}, \\ f_{B_s}/f_B &= 1.206(5). \end{aligned} \quad (35)$$

These results have very similar uncertainties to those in [9] but do contain more information.

Figure 10 gives a summary of lattice QCD results for f_B , f_{B_s} , and their ratio. It includes results from a variety of light and heavy quark formalisms for calculations that have included at least 2 flavors of quarks in the sea. The most realistic version of QCD corresponds to the results in the top box, including the values we give here, where u , d , s , and c sea quarks are incorporated. Our results have the additional advantage of including physical values for the u/d sea quarks, taking $m_u = m_d$. The results for f_B plotted in Fig. 10 correspond to a B meson made with a light quark with the u/d average mass. The grey bands show average values from [1], where there is also discussion of the effects of isospin breaking. The main message from Fig. 10 is that of good agreement between the different lattice QCD results, which is another good test of systematic uncertainties.

A similarly encouraging picture was given of the comparison of temporal vector and scalar current results for the scalar form factor for $B \rightarrow \pi$ decay in Sec. III C. The

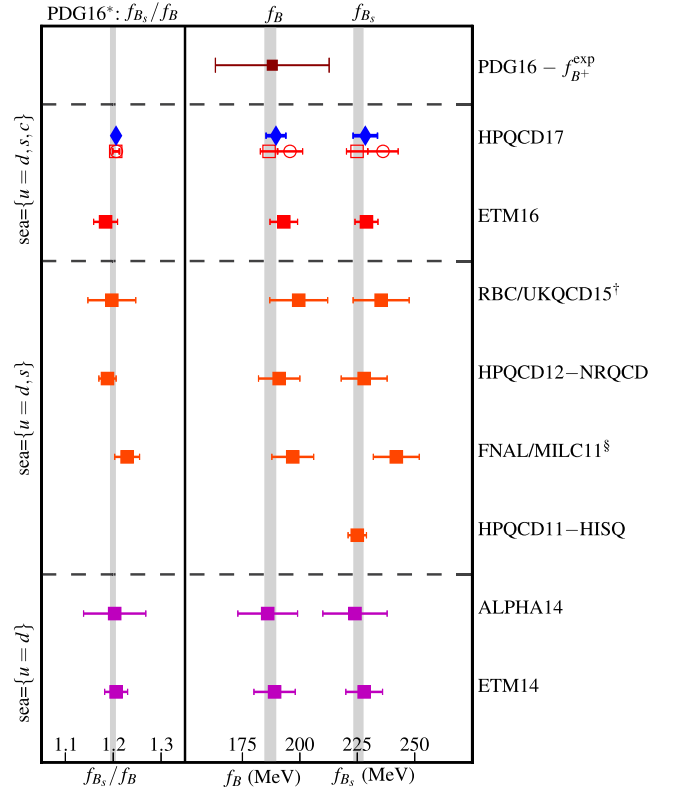


FIG. 10. A summary of lattice QCD calculations for f_B , f_{B_s} , and their ratio. The new results reported here are those for the pseudoscalar current given by the red open circles, showing good agreement with earlier results (given by red open squares) using the temporal axial current [9]. The average of these results is given by blue diamonds. Other results in this summary are taken from [36–42] and use a variety of different quark formalisms for heavy and light quarks as well as working with gluon field configurations that include different numbers of flavors of sea quarks. The results for f_B correspond to those for a light valence quark of mass equal to the average of u and d quark masses except for “RBC/UKQCD15” which correspond to the neutral $b\bar{d}$ meson and “FNAL/MILC11” which correspond to the charged $b\bar{u}$ meson. The experimental result for the charged B meson is an average from the Particle Data Group [1], as are the grey bands.

calculations compared were done at zero recoil where the π is at rest in the rest frame of the B . Here we discuss briefly the potential uses of our new method to determine the vector form factor f_+ away from the zero recoil point, where connection to experimental decay rates can be made for the determination of Cabibbo-Kobayashi-Maskawa matrix element $|V_{ub}|$.

Power counting in powers of the inverse heavy quark mass must be modified for current matrix elements away from the zero recoil point as the momentum of the light meson in the final state increases. Subleading currents that include a spatial derivative on the light quark field will have matrix elements that grow as $|\mathbf{p}'|/m_b$, and these can become relatively large compared to the leading order current if $p' > \Lambda_{\text{QCD}}$. The issue is discussed for the

NRQCD-asqtad case in [43] where ratios of the subleading matrix elements to the leading matrix elements between the B meson and a heavy pion of the spatial vector current are shown. The matrix elements for currents denoted $J_k^{(2)}$ and $J_k^{(4)}$ grow as a proportion of the leading order ($J_k^{(0)}$) matrix element as the pion momentum is increased. This is also true, although not shown there, for the matrix elements of the temporal vector current $J_0^{(2)}$. These three currents are analogous to the current $J_{A_0,\text{lat}}^{(2)}$ [Eq. (13)] considered here, in having a derivative on the light quark field; for the spatial vector there are two such currents with different γ matrix structures. Note that the matrix elements for the subleading currents that contain a derivative on the heavy-quark field show much more benign behavior, as might be expected.

The subleading currents with derivatives on the light quark field do not appear at tree level in the expansion of the continuum heavy-light current [see Eq. (19)] and so are suppressed by powers of α_s . In the NRQCD-asqtad case the α_s coefficients of these subleading currents were calculated and turned out to be small for the largest contribution, from $J_k^{(4)}$ [43]. For the NRQCD-HISQ case these coefficients are only known for the temporal vector current (see Table II [10]). As we move away from zero recoil in $B \rightarrow \pi$ decay, systematic uncertainties from these subleading currents will grow if they are not included in our nonrelativistic expansion of the continuum current. It is therefore important to work with NRQCD-HISQ currents that do include the subleading currents with derivatives on the light quark field so that accuracy can be maintained as far from zero recoil as possible.

Here we have provided a way of doing this by using the temporal vector and scalar currents [and Eqs. (29) and (30)], as used for example in calculations with purely HISQ quarks [13,14]. As we have shown, both of these continuum currents can be written as a nonrelativistic expansion in NRQCD-HISQ currents that includes terms that will become $\mathcal{O}(\alpha_s|\mathbf{p}'|/m_b)$ away from the zero recoil point. Using simple power-counting estimates these could be of

size 7% for $p' \approx 1$ GeV (double that at the zero recoil point). Dropping these terms means that there could be systematic uncertainties at this level. If the relativistic expansion instead includes these correction terms, as we show how to do here, uncertainties are then $\mathcal{O}(\alpha_s^2|\mathbf{p}'|/m_b)$ and $\mathcal{O}(\alpha_s|\mathbf{p}'|^2/m_b^2)$, which reduces them to the 3% level. This improved approach will be used in NRQCD-HISQ work on the second-generation $2+1+1$ HISQ configurations, extending [27] away from zero recoil.

It should also be noted that the expansion for the pseudoscalar heavy-light current will allow more form factors to be separated out in the analysis of B meson decays to light vectors [44,45]. Processes such as $B_s \rightarrow \phi \ell^+ \ell^-$ and $B \rightarrow K^* \ell^+ \ell^-$ provide key opportunities for stringent tests of the Standard Model [46,47] and will need increasingly accurate lattice QCD results for comparison.

ACKNOWLEDGMENTS

We are grateful to the MILC Collaboration for the use of their configurations and to R. Dowdall and B. Colquhoun for determination of the matrix elements needed in this calculation. Computing was done on the Darwin supercomputer at the University of Cambridge as part of STFC's DiRAC facility. We are grateful to the Darwin support staff for assistance. Funding for this work came from the Royal Society, the Wolfson Foundation, and STFC. C. J. M. is supported in part by the U.S. Department of Energy through Grant No. DE-FG02-00ER41132. This manuscript has been authored by Fermi Research Alliance, LLC under Contract No. DE-AC02-07CH11359 with the U.S. Department of Energy, Office of Science, Office of High Energy Physics. The United States Government retains and the publisher, by accepting the article for publication, acknowledges that the United States Government retains a nonexclusive, paid-up, irrevocable, world-wide license to publish or reproduce the published form of this manuscript, or allow others to do so, for United States Government purposes.

-
- [1] K. A. Olive *et al.* (Particle Data Group), *Chin. Phys. C* **38**, 090001 (2014).
 - [2] C. McNeile, C. Davies, E. Follana, K. Hornbostel, and G. Lepage, *Phys. Rev. D* **82**, 034512 (2010).
 - [3] C. McNeile, C. Davies, E. Follana, K. Hornbostel, and G. Lepage, *Phys. Rev. D* **85**, 031503 (2012).
 - [4] G. P. Lepage, L. Magnea, C. Nakhleh, U. Magnea, and K. Hornbostel, *Phys. Rev. D* **46**, 4052 (1992).
 - [5] A. X. El-Khadra, A. S. Kronfeld, and P. B. Mackenzie, *Phys. Rev. D* **55**, 3933 (1997).
 - [6] N. H. Christ, M. Li, and H.-W. Lin, *Phys. Rev. D* **76**, 074505 (2007).
 - [7] E. Follana, C. Davies, G. Lepage, and J. Shigemitsu (HPQCD Collaboration, UKQCD Collaboration), *Phys. Rev. Lett.* **100**, 062002 (2008).
 - [8] E. Follana, Q. Mason, C. Davies, K. Hornbostel, G. P. Lepage, J. Shigemitsu, H. Trottier, and K. Wong (HPQCD Collaboration, UKQCD Collaboration), *Phys. Rev. D* **75**, 054502 (2007).
 - [9] R. Dowdall, C. Davies, R. Horgan, C. Monahan, and J. Shigemitsu (HPQCD Collaboration), *Phys. Rev. Lett.* **110**, 222003 (2013).
 - [10] C. Monahan, J. Shigemitsu, and R. Horgan, *Phys. Rev. D* **87**, 034017 (2013).

- [11] C. T. H. Davies, C. McNeile, E. Follana, G. P. Lepage, H. Na, and J. Shigemitsu, *Phys. Rev. D* **82**, 114504 (2010).
- [12] A. Bazavov *et al.* (Fermilab Lattice and MILC Collaborations), *Phys. Rev. D* **90**, 074509 (2014).
- [13] H. Na, C. T. H. Davies, E. Follana, G. P. Lepage, and J. Shigemitsu, *Phys. Rev. D* **82**, 114506 (2010).
- [14] J. Koponen, C. T. H. Davies, G. C. Donald, E. Follana, G. P. Lepage, H. Na, and J. Shigemitsu, *arXiv:1305.1462*.
- [15] A. Bazavov *et al.*, *Phys. Rev. Lett.* **112**, 112001 (2014).
- [16] C. J. Morningstar and J. Shigemitsu, *Phys. Rev. D* **57**, 6741 (1998).
- [17] C. J. Morningstar and J. Shigemitsu, *Phys. Rev. D* **59**, 094504 (1999).
- [18] E. Dalgic, J. Shigemitsu, and M. Wingate, *Phys. Rev. D* **69**, 074501 (2004).
- [19] A. Hart, G. M. von Hippel, R. R. Horgan, and E. H. Muller, *Comput. Phys. Commun.* **180**, 2698 (2009).
- [20] G. P. Lepage, L. Magnea, C. Nakhleh, U. Magnea, and K. Hornbostel, *Phys. Rev. D* **46**, 4052 (1992).
- [21] A. Gray, I. Allison, C. T. H. Davies, E. Dalgic, G. P. Lepage, J. Shigemitsu, and M. Wingate, *Phys. Rev. D* **72**, 094507 (2005).
- [22] R. J. Dowdall *et al.* (HPQCD Collaboration), *Phys. Rev. D* **85**, 054509 (2012).
- [23] A. Bazavov *et al.* (MILC Collaboration), *Phys. Rev. D* **82**, 074501 (2010).
- [24] A. Bazavov *et al.* (MILC Collaboration), *Phys. Rev. D* **87**, 054505 (2013).
- [25] A. Hart, G. M. von Hippel, and R. R. Horgan (HPQCD Collaboration), *Phys. Rev. D* **79**, 074008 (2009).
- [26] T. C. Hammant, A. G. Hart, G. M. von Hippel, R. R. Horgan, and C. J. Monahan, *Phys. Rev. Lett.* **107**, 112002 (2011); **115**, 039901(E) (2015).
- [27] B. Colquhoun, R. J. Dowdall, J. Koponen, C. T. H. Davies, and G. P. Lepage, *Phys. Rev. D* **93**, 034502 (2016).
- [28] R. Dowdall, C. Davies, G. Lepage, and C. McNeile (HPQCD Collaboration), *Phys. Rev. D* **88**, 074504 (2013).
- [29] R. Dowdall, C. Davies, T. Hammant, and R. Horgan (HPQCD Collaboration), *Phys. Rev. D* **86**, 094510 (2012).
- [30] B. Chakraborty, C. T. H. Davies, B. Galloway, P. Knecht, J. Koponen, G. C. Donald, R. J. Dowdall, G. P. Lepage, and C. McNeile, *Phys. Rev. D* **91**, 054508 (2015).
- [31] C. Patrignani *et al.* (Particle Data Group), *Chin. Phys. C* **40**, 100001 (2016).
- [32] C. A. Dominguez, J. G. Korner, and K. Schilcher, *Phys. Lett. B* **248**, 399 (1990).
- [33] M. B. Wise, *Phys. Rev. D* **45**, R2188 (1992).
- [34] G. Burdman and J. F. Donoghue, *Phys. Lett. B* **280**, 287 (1992).
- [35] L. Wolfenstein, *Phys. Lett. B* **291**, 177 (1992).
- [36] A. Bussone *et al.* (ETM Collaboration), *Phys. Rev. D* **93**, 114505 (2016).
- [37] N. H. Christ, J. M. Flynn, T. Izubuchi, T. Kawanai, C. Lehner, A. Soni, R. S. Van de Water, and O. Witzel, *Phys. Rev. D* **91**, 054502 (2015).
- [38] H. Na, C. J. Monahan, C. T. H. Davies, R. Horgan, G. P. Lepage, and J. Shigemitsu, *Phys. Rev. D* **86**, 034506 (2012).
- [39] A. Bazavov *et al.* (Fermilab Lattice and MILC Collaborations), *Phys. Rev. D* **85**, 114506 (2012).
- [40] C. McNeile, C. T. H. Davies, E. Follana, K. Hornbostel, and G. P. Lepage, *Phys. Rev. D* **85**, 031503 (2012).
- [41] F. Bernardoni *et al.* (ALPHA Collaboration), *Phys. Lett. B* **735**, 349 (2014).
- [42] N. Carrasco *et al.* (ETM Collaboration), *J. High Energy Phys.* **03** (2014) 016.
- [43] E. Dalgic, A. Gray, M. Wingate, C. T. H. Davies, G. P. Lepage, and J. Shigemitsu, *Phys. Rev. D* **73**, 074502 (2006); **75**, 119906(E) (2007).
- [44] R. R. Horgan, Z. Liu, S. Meinel, and M. Wingate, *Phys. Rev. Lett.* **112**, 212003 (2014).
- [45] R. R. Horgan, Z. Liu, S. Meinel, and M. Wingate, *Phys. Rev. D* **89**, 094501 (2014).
- [46] R. Aaij *et al.* (LHCb Collaboration), *J. High Energy Phys.* **07** (2013) 084.
- [47] R. Aaij *et al.* (LHCb Collaboration), *J. High Energy Phys.* **06** (2014) 133.